Two-mode theory of vortex stability in multicomponent Bose-Einstein condensates

Víctor M. Pérez-García and Juan J. García-Ripoll
Departamento de Matemáticas, Escuela Técnica Superior de Ingenieros Industriales, Universidad de Castilla-La Mancha, 13071 Ciudad Real, Spain

(Received 16 December 1999; revised manuscript received 20 March 2000; published 8 August 2000)

We study the stability and dynamics of vortices in two-species condensates using a two-mode model. The recent experimental results obtained at JILA [M. R. Matthews *et al.*, Phys. Rev. Lett. **83**, 2498 (1999)] and recent numerical simulations based on the Gross-Pitaevskii equations are explained using this simple model. We also make an exhaustive analysis of the stability properties of the system when the relative populations of the two species and/or their relative scattering lengths are changed and prove that stabilization of otherwise unstable configurations can be attained by controlling the relative population of both species.

PACS number(s): 03.75.Fi, 67.57.Fg, 67.90.+z

I. INTRODUCTION

Vortices appear in many different physical contexts ranging from classical phenomena such as fluid mechanics [1] and nonlinear optics [2] to purely quantum phenomena such as superconductivity [3] and superfluidity [4].

A vortex is the simplest topological defect one can construct [5], and it is characterized by the fact that in any closed path around a vortex, the phase of the involved field undergoes an integer multiple of 2π winding. When the phase jump is $\pm 2\pi$, then it implies the stabilization of a zero value of the field placed in what is called the vortex core, i.e., one extreme of the line that joins the discontinuities of the phase. This stabilization is due to topological constraints since removing the phase singularity implies an effect on the boundaries of the system that is difficult to achieve using local perturbations.

The concept of a vortex is central to our understanding of superfluidity and quantized flow. This is the reason why the experimental realization of Bose-Einstein condensates (BEC) with ultracold atomic gases [6] has triggered the analysis of vortices. The main goals in this field have been the generation [7,8], detection [9], and stability properties [10–14] of vortices.

Although most of the theoretical effort has concentrated on single condensate systems, the first experimental realization of BEC vortices [15] was attained following the proposal of Ref. [16] with a two-species ^{87}Rb condensate. The two species correspond to two different hyperfine levels of ^{87}Rb, denoted by $|1\rangle$ and $|2\rangle$. From Ref. [15], we know that while one may build two possible configurations with a unit charge vortex, only one of them is stable. The stable configuration corresponds to the vortex placed on the $|1\rangle$ state, namely, the one with the largest scattering length. The configuration with the vortex placed in the $|2\rangle$ state, on the other hand, leads to some kind of instability. To simplify the reading of this paper, we will use in what follows a shorthand notation for these states: $|1,0\rangle$ will refer to the state in which the vortex is hosted by $|1\rangle$, and $|0,1\rangle$, the state with the vortex in $|2\rangle$.

In a recent work [17], we have used numerical simulations to show that the instability of state $|0,1\rangle$ is purely dynamical and can be understood within the framework of mean-field theories for the double condensate system. A consequence of the analysis is that, if dissipation is small, the instability mechanism does not lead to expulsion of the vortex from condensate, but to the establishment of a complex state in which the phase singularity periodically moves from one specie to the other.

The purpose of this paper is twofold. First we want to understand the mechanism of the instability. In this sense, our paper will confirm the results from [17] by proving for this system that the instability arises even with the least number of degrees of freedom. The second target of the paper is to learn what happens with the $|1,0\rangle$ and $|0,1\rangle$ configurations when we vary the relative populations of both species. The results are also applicable to other multiple condensate systems where the set of scattering lengths is different from those of rubidium.

To ease the analysis and get an intuitive physical interpretation, we make most of the analysis using a simplified two-mode model that is exact in the linear limit but provides good qualitative predictions that are in agreement with the experiment of Ref. [15] and the numerics of Ref. [17]. These results will be further confirmed by numerical simulations of the full three-dimensional mean field equations ruling the phenomenon.

Our plan is as follows: In Sec. II we present our problem in a suitable form and obtain the reduced set of equations for the two-mode model. In Sec. III we apply the two-mode model to the system discussed in the previous analysis [15,17]. In Sec. IV we make a complete stability analysis of the relevant configurations and make some predictions that are experimentally testable. Finally, in Sec. V we summarize our conclusions.

II. THE MODEL

A. Mean-field equations for the two-condensate system

In this work, we will use the zero-temperature approximation, in which collisions between the condensed and noncondensed atomic clouds are neglected. In the two-species case, this leads to a pair of coupled Gross-Pitaevskii equations (GPE) for the condensate wave functions of each species:

$$i\hbar\frac{\partial}{\partial t}\Psi_1=\left[-\frac{\hbar^2\nabla^2}{2m}+V_1+U_{11}|\Psi_1|^2+U_{12}|\Psi_2|^2\right]\Psi_1, \tag{1a}$$

$$i\hbar\frac{\partial}{\partial t}\Psi_2=\left[-\frac{\hbar^2\nabla^2}{2m}+V_2+U_{21}|\Psi_1|^2+U_{22}|\Psi_2|^2\right]\Psi_2, \tag{1b}$$

where $U_{ij}=4\pi\hbar^2 a_{ij}/m$ are constants controlling the nonlinear behavior, which are proportional to the the *s*-wave scattering lengths of $1-1$, (a_{11}), $2-2$ (a_{22}), and $1-2$ (a_{12}) binary collisions.

To simplify the formalism, we assume that both trapping potentials are concentric and spherically symmetric, $V_1(\vec{r})=V_2(\vec{r})=\frac{1}{2}m\omega^2 r^2$, just like in the experiment. The consideration of the differences between V_1 and V_2 does not add new physics to the model as it will be discussed in detail later.

Next we change to a new set of units based on the trap characteristic length $a_0=\sqrt{\hbar/m\omega}$ and period $\tau=1/\omega$ defined as $x\to x/a_0, t\to t/\tau$, $u_{ij}=4\pi N_j a_{ij}/a_0$, and $\Psi_j(\mathbf{x})=N_j\psi_j(\mathbf{x})$. Equations (1) conserve the number of particles on each hyperfine level and so we may choose

$$\int|\psi_1(\vec{r})|^2=\int|\psi_2(\vec{r})|^2\equiv 1. \tag{2}$$

This choice implies that the particle number of each species appears on the nonlinear coefficients u_{ij}.

The experimental results [15] and our previous theoretical analysis [17] correspond to systems in which the number of particles is the same for each component, $N_1=N_2=N$, but in general one could allow any proportion between the populations of the different levels.

With the previous rescaling, the GPE for the multicomponent system read

$$i\frac{\partial}{\partial t}\psi_1=\left[-\frac{1}{2}+\frac{1}{2}r^2+u_{11}|\psi_1|^2+u_{12}|\psi_2|^2\right]\psi_1, \tag{3a}$$

$$i\frac{\partial}{\partial t}\psi_2=\left[-\frac{1}{2}+\frac{1}{2}r^2+u_{21}|\psi_1|^2+u_{22}|\psi_2|^2\right]\psi_2. \tag{3b}$$

Since the realistic values of ^{87}Rb scattering lengths are in the proportion $a_{11}:a_{12}:a_{22}=1.00:0.97:0.94$ [18], the coefficients of the matrix of nonlinear coefficients satisfy the relations $u_{11}/u_{12}=a_{11}N_1/a_{12}N_2, u_{21}/u_{22}=a_{12}N_1/a_{22}N_2$, which means that except for the particular case in which $N_1=N_2=N$, this matrix is nonsymmetric. In terms of the population imbalance $\beta=N_2/N_1$, and for a fixed total number of particles the matrix can be written as

$$\begin{pmatrix}u_{11}&u_{12}\\u_{21}&u_{22}\end{pmatrix}=\frac{4\pi a_{11}N}{a_0}\begin{pmatrix}\frac{1.00}{1+\beta}&\frac{0.97\beta}{1+\beta}\\\frac{0.97}{1+\beta}&\frac{0.94\beta}{1+\beta}\end{pmatrix}. \tag{4}$$

B. Derivation of a two-mode model

In our previous work [17], we worked on the basis of the full GPE to prove the instability of the $|0,1\rangle$ stationary solution, as well as the stability of the $|1,0\rangle$ state for typical experimental conditions. That stability analysis demonstrated that the instability was mediated by the growth of a core mode that pushes the vortex out of the condensed cloud. This fact makes plausible the description of the two-condensate dynamics by the use of only two modes for each level: one corresponds to a centered vortex and the other to a nodeless or *core* mode. This approach, which corresponds to retaining the stationary plus active modes and has been used successfully in the analysis of other nonlinear problems [19], should work at least in the linear regime in which perturbations are small.

Mathematically, the idea is to approximate:

$$\psi_1(\mathbf{x})\simeq a(t)\psi_{g1}(\mathbf{x})+b(t)\psi_{e1}(\mathbf{x}), \tag{5a}$$

$$\psi_2(\mathbf{x})\simeq c(t)\psi_{g2}(\mathbf{x})+d(t)\psi_{e2}(\mathbf{x}). \tag{5b}$$

Here, $\psi_{gj}(x)$ is the spatial wave function of the ground state or core mode for each specie, $|j\rangle$, and $\psi_{ej}(x)$ corresponds to a representation of the single vortex wave function. This approximation implies some loss of information about the dynamics but it is not essential for our results, as will be shown later [20].

We can also relate this idea and its representation [Eq. (5)] to a recent work on the dynamics of a single condensate [8], with the difference that the modes from Ref. [8] are fully nonlinear and depend on their populations $\{a,b,c,d\}$ (so there is no simple analytical expression for them). Our approach is simpler but, as we will see, the two-mode ansatz reflects the essentials of the dynamics with good accuracy.

ψ_g, ψ_e can be chosen as any approximation to the ground and first excited states of the single-species equations, provided they are orthogonal, which automatically is guaranteed if ψ_e has a vortex and ψ_g does not. Our choice will be to use the eigenfunctions of the *d*-dimensional harmonic oscillator that are the exact solutions in the linear case and allow simple manipulation since their analytic form is known:

$$\psi_g(\mathbf{x})=\left(\frac{1}{\pi}\right)^{d/2}e^{-r^2/2}, \tag{6a}$$

$$\psi_e(\mathbf{x})=\left(\frac{2}{d\pi}\right)^{d/2}re^{-r^2/2}e^{i\theta}. \tag{6b}$$

Other choices are feasible with the only change of several coefficients related to integrals involving ψ_g and ψ_e, as will be discussed later.

In our treatment, we will consider simultaneously the two- (2D) and three-dimensional configurations. It was shown in a previous work concerning single condensates [12] that the transition from a spherical trap to a pancake preserves the shape and number of unstable modes. Our present analysis applies equally to the simplified 2D situation used in Ref. [17] as well as to the full 3D problem and

proves that there are no essential differences between the two- and three-dimensional models for the type of phenomena described here.

Inserting the ansatz from Eq. (5) into the GP equation (3) and projecting on ψ_{gj} and ψ_{ej} one obtains the following set of coupled nonlinear ordinary differential equations:

$$i\dot{a} = -aE_g + u_{11}a(\gamma_1|a|^2 + 2\gamma_2|b|^2) + u_{12}a(\gamma_1|c|^2 + \gamma_2|d|^2) + u_{12}\gamma_2 bcd^*, \tag{7a}$$

$$i\dot{b} = -bE_e + u_{11}b(\gamma_3|b|^2 + 2\gamma_2|a|^2) + u_{12}b(\gamma_2|c|^2 + \gamma_3|d|^2) + u_{12}\gamma_2 ac^*d, \tag{7b}$$

$$i\dot{c} = -cE_g + u_{22}c(\gamma_1|c|^2 + 2\gamma_2|d|^2) + u_{21}c(\gamma_1|c|^2 + \gamma_2|d|^2) + u_{21}\gamma_2 dab^*, \tag{7c}$$

$$i\dot{d} = -dE_e + u_{22}d(\gamma_3|d|^2 + 2\gamma_2|c|^2) + u_{21}d(\gamma_2|a|^2 + \gamma_3|b|^2) + u_{21}\gamma_2 ca^*b. \tag{7d}$$

Here, $\gamma_1 = (|\psi_g|^2, |\psi_g|^2)$, $\gamma_2 = (|\psi_g|^2, |\psi_e|^2)$, $\gamma_3 = (|\psi_e|^2, |\psi_e|^2)$, and $E_g = (\psi_g, H_0\psi_g), E_e = (\psi_e, H_0\psi_e)$ being $H_0 = -\frac{1}{2}\triangle + \frac{1}{2}r^2$. For our particular choice of ψ_g and ψ_e, the values of these coefficients are $\gamma_1^{2d} = 1/2\pi, \gamma_2^{2d} = 1/4\pi$, $\gamma_3^{2d} = 1/4\pi, E_g^{2D} = 1, E_e^{2D} = 2$, $\gamma_1^{3d} = 1/(2\pi)^{3/2}, \gamma_2^{3d} = 1/2(2\pi)^{3/2}$, $\gamma_3^{3d} = 5/12(2\pi)^{3/2}$, $E_g^{3D} = 3/2$, and $E_e^{3D} = 5/2$.

If the trapping potentials V_1 and V_2 are not considered to be equal, then the shapes of the modes ψ_g and ψ_e in $|1\rangle$ and $|2\rangle$ are different. However, the only difference with respect to our present treatment is on the precise numerical value of the coefficients, which is not essential for what follows. The same happens when other functions are considered to represent the ground and first excited state instead of harmonic-oscillator basis functions.

Equations (3) satisfy discrete conservation laws corresponding to the number of particles of each species and angular momentum,

$$|a|^2 + |b|^2 = 1, \tag{8a}$$

$$|c|^2 + |d|^2 = 1, \tag{8b}$$

$$|b|^2 + |d|^2 = L_0, \tag{8c}$$

L_0 being the angular momentum of the initial data. There is another conservation law for the energy that is not relevant to our purposes.

It is convenient to change to a modulus-phase representation given by $a = \rho_a e^{i\phi_a}, b = \rho_b e^{i\phi_b}, c = \rho_c e^{i\phi_c}, d = \rho_d e^{i\phi_d}$. Equations (7) then become

$$\dot{\rho}_a = u_{12}\gamma_2\rho_b\rho_c\rho_d \sin(\phi_b + \phi_c - \phi_d - \phi_a), \tag{9a}$$

$$\dot{\phi}_a = E_g - u_{11}(\gamma_1\rho_a^2 + 2\gamma_2\rho_b^2) - u_{12}(\gamma_1\rho_c^2 + \gamma_2\rho_d^2) - u_{12}\gamma_2\frac{\rho_b\rho_c\rho_d}{\rho_a}\cos(\phi_b + \phi_c - \phi_d - \phi_a), \tag{9b}$$

$$\dot{\rho}_b = u_{12}\gamma_2\rho_a\rho_c\rho_d \sin(\phi_a + \phi_d - \phi_a - \phi_c), \tag{9c}$$

$$\dot{\phi}_b = E_e - u_{11}(\gamma_3\rho_b^2 + 2\gamma_2\rho_a^2) - u_{12}(\gamma_2\rho_c^2 + \gamma_3\rho_d^2) - u_{12}\gamma_2\frac{\rho_a\rho_c\rho_d}{\rho_b}\cos(\phi_d + \phi_a - \phi_c - \phi_b), \tag{9d}$$

$$\dot{\rho}_c = u_{21}\gamma_2\rho_b\rho_a\rho_d \sin(\phi_b + \phi_c - \phi_d - \phi_a), \tag{9e}$$

$$\dot{\phi}_c = E_g - u_{22}(\gamma_1\rho_c^2 + 2\gamma_2\rho_d^2) - u_{21}(\gamma_1\rho_a^2 + \gamma_2\rho_b^2) - u_{21}\gamma_2\frac{\rho_b\rho_a\rho_d}{\rho_c}\cos(\phi_b + \phi_c - \phi_d - \phi_a), \tag{9f}$$

$$\dot{\rho}_d = u_{21}\gamma_2\rho_a\rho_b\rho_c \sin(\phi_d + \phi_a - \phi_a - \phi_c), \tag{9g}$$

$$\dot{\phi}_d = E_e - u_{22}(\gamma_3\rho_d^2 + 2\gamma_2\rho_c^2) - u_{21}(\gamma_2\rho_a^2 + \gamma_3\rho_b^2) - u_{21}\gamma_2\frac{\rho_a\rho_c\rho_b}{\rho_d}\cos(\phi_d + \phi_a - \phi_c - \phi_b). \tag{9h}$$

Despite the apparent complexity of this system, it is easy to prove that the four phase variables can be reduced to a single one given by $\Phi = \phi_b + \phi_c - \phi_a - \phi_d$. The dynamics on these new variables is ruled by

$$\dot{\rho}_a = u_{12}\gamma_2\rho_b\rho_c\rho_d \sin\Phi, \tag{10a}$$

$$\dot{\rho}_b = -u_{12}\gamma_2\rho_a\rho_c\rho_d \sin\Phi, \tag{10b}$$

$$\dot{\rho}_c = -u_{21}\gamma_2\rho_b\rho_a\rho_d \sin\Phi, \tag{10c}$$

$$\dot{\rho}_d = u_{21}\gamma_2\rho_a\rho_b\rho_c \sin\Phi, \tag{10d}$$

$$\dot{\Phi} = \gamma_a\rho_a^2 + \gamma_b\rho_b^2 + \gamma_c\rho_c^2 + \gamma_d\rho_d^2 + \gamma_2\left[u_{12}\left(\frac{\rho_b\rho_c\rho_d}{\rho_a} - \frac{\rho_a\rho_c\rho_d}{\rho_b}\right) + u_{21}\left(\frac{\rho_b\rho_c\rho_a}{\rho_d} - \frac{\rho_a\rho_b\rho_d}{\rho_c}\right)\right]. \tag{10e}$$

We have now five ordinary differential equations in Eq. (10) plus four conservation laws, which means that the system can be (at least formally) integrated. This fact excludes the possibility of chaotic behavior in the system.

Equations (10) can be further simplified by defining density variables related to ρ_j^2 and $X = \rho_a\rho_b\rho_c\rho_d$ and using the conservation laws. We will not follow this route since all the simplified models such as the one presented in Eqs. (10) have singularities when any of the densities is zero. This fact makes the new equations useless for a stability analysis, since the stationary states are singular solutions of these systems.

III. DYNAMICS IN THE PHYSICALLY RELEVANT CASE

The experimental configurations first described in [15] and later numerically studied in [17] correspond to unit charge vortices in either $|1\rangle$ or $|2\rangle$, with the constraint that

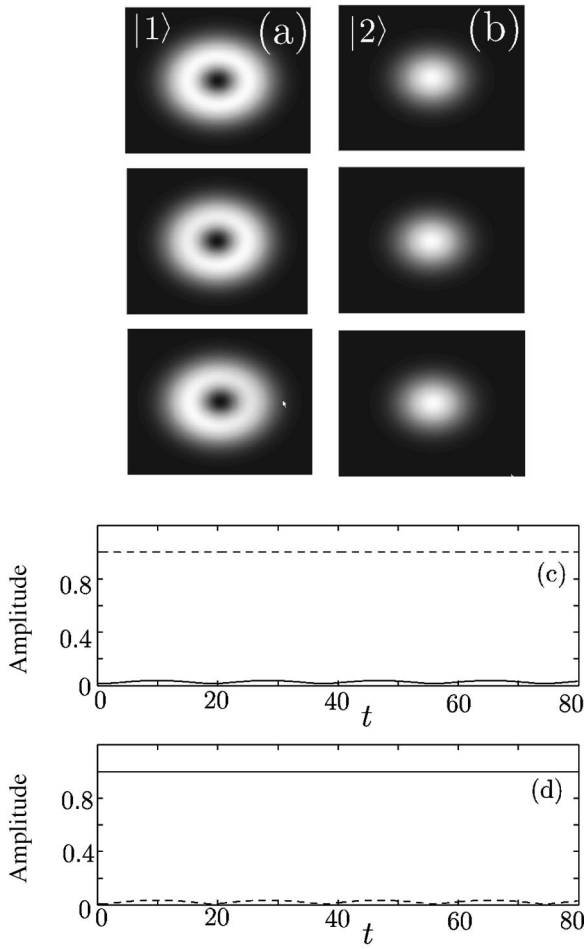

FIG. 1. Stability of the configuration $|1,0\rangle$. Snapshots of the spatial density of (a) $|1\rangle$ and (b) $|2\rangle$. Evolution the amplitudes of the modes with time (c) $|a|$ (solid line) and $|b|$ (dashed line); (d) $|c|$ (solid line) and $|d|$ (dashed line).

the populations of both hyperfine levels are equal, i.e., $\beta=1$ and $u_{21}=u_{12}$. It is interesting to study the dynamics under small perturbations of the initial data $a(0)=0,b(0)=1,c(0)=1,d(0)=0$, which physically corresponds to the stationary state $|1,0\rangle$, and $a(0)=1,b(0)=0,c(0)=0,d(0)=1$, which corresponds to $|1,0\rangle$. Both initial data correspond to two different periodic solutions of the amplitude equations (7), which are

$$a(t)=0,b(t)=e^{i(E_e-u_{11}\gamma_3-u_{12}\gamma_2)t},$$

$$c(t)=e^{i(E_g-u_{22}\gamma_1-u_{21}\gamma_2)t},\quad d(t)=0; \tag{11a}$$

$$a(t)=e^{i(E_e-u_{11}\gamma_1-u_{12}\gamma_2)t},\quad b(t)=0,$$

$$c(t)=0,\quad d(t)=e^{i(E_g-u_{22}\gamma_3-u_{21}\gamma_2)t}. \tag{11b}$$

To have a clear picture of what is going on, we have first simulated the dynamics of these states when small perturbations are added to the initial data. The results are summarized in Figs. 1–4. It is clear from Fig. 1 that the configuration that has a vortex in $|1\rangle$ is dynamically stable. However, when a vortex is placed in $|2\rangle$, an instability develops and the response to small perturbations is to transfer the vortex to $|1\rangle$ and start a periodic transfer dynamics. The snapshots of the density during the destabilization process are shown in Fig. 2. In Fig. 3, we show how the phase singularity in $|2\rangle$ spirals out of the system while a phase singularity appears in $|1\rangle$ and occupies the center of the atomic cloud [21]. This dynamics is recurrent as can be seen from the evolution of the relevant variables (Fig. 4).

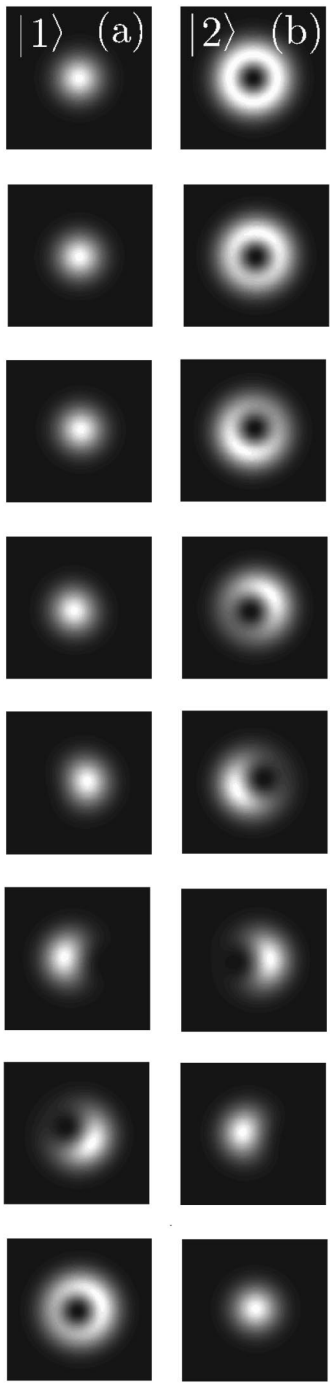

FIG. 2. Snapshots of the evolution of an unstable vortex (state $|0,1\rangle$). Evolution of the spatial density of (a) $|1\rangle$ and (b) $|2\rangle$.

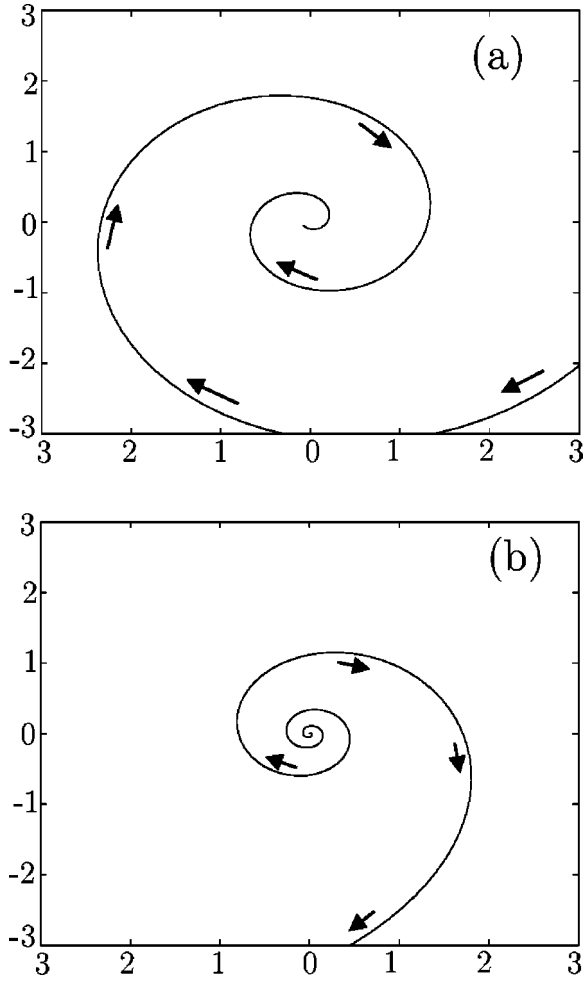

FIG. 3. Evolution of the position of the phase singularity corresponding to the simulation shown in Fig. 2. (a) Phase singularity in $|1\rangle$. (b) Phase singularity in $|2\rangle$.

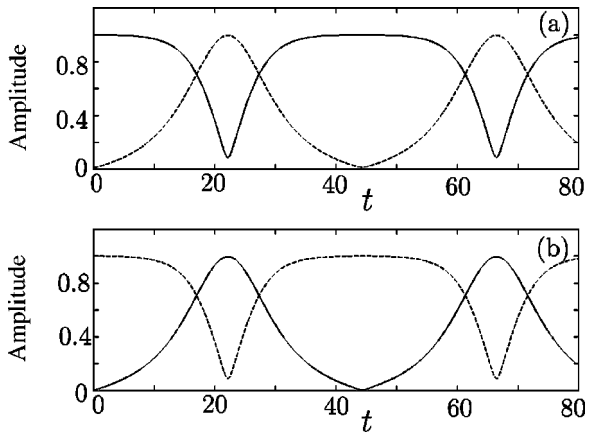

FIG. 4. Evolution of the amplitudes of the modes (a) $|a|$ (dashed line) and $|b|$ (solid line); (b) $|c|$ (dashed line) and $|d|$ (solid line). The simulation is done adding a random perturbation to the configuration with vortex in $|2\rangle$, i.e., $a(0)=e^{ir_2}\sqrt{1-\epsilon_1^2}$, $b(0)=\epsilon_1 e^{ir_3}$, $c(0)=\epsilon_2 e^{ir_4}$; $d(0)=\sqrt{1-\epsilon_2^2}$. ϵ_1 and ϵ_2 are random numbers uniformly distributed between 0 and 0.02. r_j are random numbers uniformly distributed between 0 and 1.

IV. STABILITY THEORY

A. Problem statement

Our numerical simulations of the reduced system (7) show that in the equal population case, $N_1=N_2=N$, and for arbitrary nonlinearities only one of the possible stationary states of the system is stable. It is our purpose in this section to make a complete analysis of the stability of the system for any proportion of the populations $\beta=N_1/N_2$ and any value of the nonlinear coefficients (e.g., total number of particles N and scattering lengths a_{ij}). These results could be specially relevant to predict the existence of stable vortex states for a specific multiple-condensate system. For the case of ^{87}Rb, the results can be applied to study the possibility of stabilizing different configurations.

B. Stability of the state $|1,0\rangle$

When a vortex is placed in $|1\rangle$, the resulting stationary state is a periodic orbit described by Eq. (11a). Its direct stability analysis using Eqs. (7) would lead to time-dependent perturbation equations that should be analyzed using Floquet's theory. A way to partially circumvent this situation is to change to the rotating frame of reference defined by

$$\tilde{a}=ae^{-i(E_g-u_{22}\gamma_1-u_{21}\gamma_2)t}, \tag{12a}$$

$$\tilde{b}=be^{-i(E_e-u_{11}\gamma_3-u_{12}\gamma_2)t}, \tag{12b}$$

$$\tilde{c}=ce^{-i(E_g-u_{22}\gamma_1-u_{21}\gamma_2)t}, \tag{12c}$$

$$\tilde{d}=de^{-i(E_e-u_{11}\gamma_3-u_{12}\gamma_2)t}. \tag{12d}$$

Using these new variables, the equations are

$$\dot{\tilde{a}}=i(\gamma_1u_{22}+\gamma_2u_{21})\tilde{a}-iu_{11}\tilde{a}(\gamma_1|\tilde{a}|^2+2\gamma_2|\tilde{b}|^2) -iu_{12}\tilde{a}(\gamma_1|\tilde{c}|^2+\gamma_2|\tilde{d}|^2)-iu_{12}\gamma_2\tilde{b}\tilde{c}\tilde{d}^*, \tag{13a}$$

$$\dot{\tilde{b}}=i(\gamma_3u_{11}+\gamma_2u_{12})\tilde{b}-iu_{11}\tilde{b}(\gamma_3|\tilde{b}|^2+2\gamma_2|\tilde{a}|^2) -iu_{12}\tilde{b}(\gamma_2|\tilde{c}|^2+\gamma_3|\tilde{d}|^2)-iu_{12}\gamma_2\tilde{a}\tilde{c}^*\tilde{d}, \tag{13b}$$

$$\dot{\tilde{c}}=i(\gamma_1u_{22}+\gamma_2u_{21})\tilde{c}-iu_{22}\tilde{c}(\gamma_1|\tilde{c}|^2+2\gamma_2|\tilde{d}|^2) -iu_{21}\tilde{c}(\gamma_1|\tilde{c}|^2+\gamma_2|\tilde{d}|^2)-iu_{21}\gamma_2\tilde{d}\tilde{a}\tilde{b}^*, \tag{13c}$$

$$\dot{\tilde{d}}=i(\gamma_3u_{11}+\gamma_2u_{21})\tilde{d}-iu_{22}\tilde{d}(\gamma_3|\tilde{d}|^2+2\gamma_2|\tilde{c}|^2) -iu_{21}\tilde{d}(\gamma_2|\tilde{a}|^2+\gamma_3|\tilde{b}|^2)-iu_{21}\gamma_2\tilde{c}\tilde{a}^*\tilde{b}. \tag{13d}$$

The stationary solution is an equilibrium point of Eqs. (13): $\tilde{a}_0=0,\tilde{b}_0=1,\tilde{c}_0=1,\tilde{d}_0=0$. To study its stability, we linearize Eqs. (13) around the equilibrium point and define the perturbations through

$$\tilde{a}=\tilde{a}_0+\delta_a(t), \tag{14a}$$

$$\tilde{b}=\tilde{b}_0+\delta_b(t), \tag{14b}$$

$$\tilde{c}=\tilde{c}_0+\delta_c(t), \tag{14c}$$

$$\tilde{d}=\tilde{d}_0+\delta_d(t). \tag{14d}$$

The new evolution laws are

$$\dot{\delta}_a=i\Delta_a\delta_a-iu_{12}\gamma_2\delta_d^*, \tag{15a}$$

$$\dot{\delta}_b=0, \tag{15b}$$

$$\dot{\delta}_c=0, \tag{15c}$$

$$\dot{\delta}_d=i\Delta_d\delta_d-iu_{21}\gamma_2\delta_a^*, \tag{15d}$$

where $\Delta_a=u_{22}\gamma_1+u_{21}\gamma_2-2\gamma_2u_{11}-\gamma_1u_{12}$, $\Delta_d=u_{11}\gamma_3+u_{12}\gamma_2-2u_{22}\gamma_2-u_{21}\gamma_3$. The perturbations for $\tilde{b}$ and $\tilde{c}$ have a neutral behavior because their evolution is ruled by quadratic terms. If we write the equations for the perturbations and their complex conjugates to obtain the full stability spectrum, we have

$$\frac{d}{dt}\begin{pmatrix}\delta_a\\ \delta_b^*\\ \delta_d\\ \delta_d^*\end{pmatrix}=i\begin{pmatrix}\Delta_a & 0 & 0 & -u_{12}\gamma_2\\ 0 & -\Delta_a & u_{12}\gamma_2 & 0\\ 0 & -u_{21}\gamma_2 & \Delta_d & 0\\ u_{21}\gamma_2 & 0 & 0 & -\Delta_d\end{pmatrix}\begin{pmatrix}\delta_a\\ \delta_b^*\\ \delta_d\\ \delta_d^*\end{pmatrix}. \tag{16}$$

The eigenvalues of this matrix can be obtained analytically, the result being

$$\lambda_{1,2}=i\left[\frac{\Delta_a-\Delta_d}{2}\pm\frac{1}{2}\sqrt{(\Delta_a+\Delta_d)^2-4\gamma_2^2u_{21}u_{12}}\right], \tag{17a}$$

$$\lambda_{3,4}=i\left[\frac{\Delta_a+\Delta_d}{2}\pm\frac{1}{2}\sqrt{(\Delta_a+\Delta_d)^2-4\gamma_2^2u_{21}u_{12}}\right]. \tag{17b}$$

There is only one stability condition, which is $|\Delta_a+\Delta_d|>2\gamma_2\sqrt{u_{21}u_{12}}$. Since the parameters Δ_j are functions of γ_j, which depend on the dimensionality and on the shape of the trial states, we must separate now the results for the 2D and 3D cases. In the two-dimensional case, we obtain

$$u_{11}+u_{12}>2\sqrt{u_{21}u_{12}}, \tag{18}$$

while for the three-dimensional setup the condition is

$$\frac{7}{6}u_{11}-\frac{1}{6}u_{21}+u_{12}>2\sqrt{u_{21}u_{12}}. \tag{19}$$

Taking into account the fact that the numerical values of a_{11} and a_{12} are very close, we find that Eqs. (18) and (19) are indeed very similar. This is why we will use one of them, Eq. (18), for the subsequent analysis. If we write the inequalities in terms of β and use the scattering length values of ^{87}Rb, we obtain the following stability condition:

$$\frac{a_{11}}{a_{12}}+\beta>2\sqrt{\beta}. \tag{20}$$

For rubidium, inequality (20) is always satisfied, which proves that the configuration with a vortex in $|1\rangle$ is always linearly stable regardless of the relative population of each specie, β. This is consistent with the results from Refs. [15,17] that show the stability of the experimental configuration with a vortex in $|1\rangle$.

It is also remarkable that the stability properties of this model do not depend on the total number of particles but only on the relation between the populations. The stability properties also depend essentially on the scattering lengths, which in our case are fixed since we are dealing with specific hyperfine levels of Rb atoms.

C. Stability of state $|0,1\rangle$

The stability analysis of configuration $|0,1\rangle$, which corresponds to initial data $a_0=1,b_0=0,c_0=0,d_0=1$, is completely equivalent to the previous one. In fact, arguments of symmetry imply that the result should be formally equivalent with only an exchange of indices $1\leftrightarrow2$, i.e., the stability condition now reads

$$\frac{a_{22}}{a_{21}}\beta+1>2\sqrt{\beta}. \tag{21}$$

This inequality is not verified for a certain range of β values. Solving the algebraic equation for β, one finds the critical values

$$\frac{1}{\beta_c}=\left(\frac{N_1}{N_2}\right)_c=2-\frac{a_{22}}{a_{12}}\pm\sqrt{1-\frac{a_{22}}{a_{21}}}. \tag{22}$$

For the case of ^{87}Rb, this formula says that the unstable range is a finite one: $\beta\in[0.73,1.49]$. This result is interesting since it means that there are choices of the population imbalance β that allow the stabilization of the vortex in $|2\rangle$. We have analyzed the ratio of angular momentum transfer from component $|2\rangle$ to $|1\rangle$ as a function of β from numerical simulations of Eqs. (7). The results are presented in Fig. 5. This is one of the main results of the paper and a prediction that can be experimentally tested and has already been numerically proved (see below).

D. Nonlinear stability analysis

Even though the linear stability analysis presents some evidences in favor of stability, it is not completely conclusive. To give a full answer to the question, a fully nonlinear stability analysis should be desirable, and this subject, which is quite technical and difficult, will be the subject of a future work.

Nevertheless there are indications that the stable configuration $|1,0\rangle$ should be sensitive to appropriate small finite amplitude perturbations. The argument is very simple. According to Fig. 4(b), when the vortex is almost completely transferred to state $|1\rangle$ (for a time of about 20 time units), we

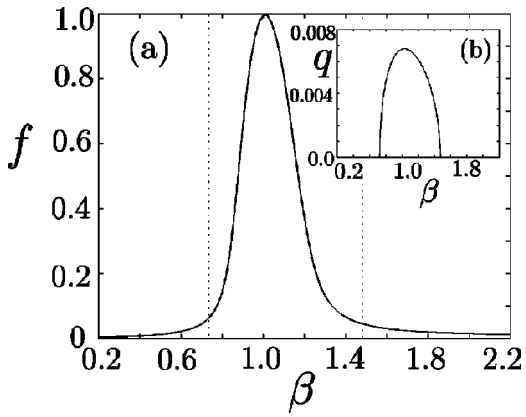

FIG. 5. Angular momentum transfer as a function of β. All the angular momentum is put initially at component $|2\rangle$. (a) We simulate the dynamics and plot the maximum over a time which captures the essentials of the dynamics of the fraction of angular momentum transferred to component $|1\rangle$, f, which is a measure of the instability, as a function of β. The vertical lines mark the points where the stability analysis predicts instability of the configurations. (b) Value of the real part of the eigenvalues leading to instability $\lambda = 4\pi N a_{11} q/a_0$.

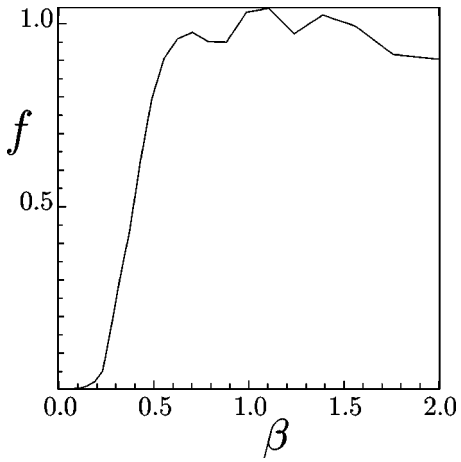

FIG. 6. Angular momentum transfer as a function of the number of particles in the second component, N_2, for a fixed sum $N=N_1+N_2=2\times10^5$. All the angular momentum is put initially at component $|2\rangle$, which is slightly displaced and then simulated according to Eq. (1). For N_2 of about 3–4 times N_1 the instability is suppressed.

are in a configuration that is close to the stable state $|1,0\rangle$, but which is actually unstable. In fact, we have added finite amplitude perturbations to the configuration $|1,0\rangle$ and found that a periodic transfer dynamics is also induced that is very similar to the dynamics of $|2,0\rangle$. The main difference is that $|1,0\rangle$ is linearly stable, which makes this configuration more robust but yet not completely stable.

E. Comparison of the predictions with simulations of the full GPE

The main results of this paper are the stability properties of the $|1,0\rangle$ and $|0,1\rangle$ states and the prediction of how to stabilize the second one by varying the relative population of the $|1\rangle$ and $|2\rangle$ components.

The first result was already obtained in [17] using numerical simulations and a linear stability analysis of the full Gross-Pitaevskii equations. Regarding the second prediction, we have verified the possibility of stabilizing the state $|0,1\rangle$ using numerical simulations of Eq. (1). In our simulations, a $|0,1\rangle$ configuration is subject to *finite* perturbations that involve the displacement of the vortex and sometimes a change of the dimensions of the cloud. By performing the same experiments over a suitable range of populations of each component while keeping the sum N_1+N_2 constant, we have obtained pictures similar to the one in Fig. 6. There we see that up from a certain population of the unstable component, the transfer of the vortex is inhibited. Although it is remarkable that the range of stabilization is smaller, the order of magnitude is similar to the one from the two-mode model. A better quantitative agreement can probably be obtained by using as radial basis functions the stationary solutions of the nonlinear GPE that resemble better the actual shape of the clouds, or even by moving to a four-mode model in which $|1\rangle$ and $|2\rangle$ are represented by different pairs of functions.

The large β region cannot be described using a two-mode model. The reason is that for $\beta\geqslant2$ then we fall into the spatiotemporally chaotic regime described in [17]. Thus the predictions of the inhibition of the instability can only be trusted when $\beta<1$ and have no sense for large β. In any case, it is striking that such a simple model is able to capture, at least for $\beta<1$, the essentials of the dynamical behavior and to predict the existence of the inhibition of the transfer of the vortex from $|2\rangle$ to $|1\rangle$.

V. CONCLUSIONS AND DISCUSSION

To summarize the work presented in this paper, we have completed the task of analyzing stability properties of vortices in double ^{87}Rb condensates, although our theory is much more general and can be applied to any two (multiple) condensate system. Our treatment is based on a simplified two-mode model that captures many of the relevant dynamical features of the problem.

We have attained several goals in this work. First, the stability results of Refs. [15,17] are reproduced for the $N_1=N_2$ case. Second, the instability mechanism consisting in vortex exchange between the two species is supported and described in detail here. Third, we raise a new prediction that consists of the fact that population imbalances can stabilize vortices in $|2\rangle$ states and also prove that vortices in $|1\rangle$ can be destabilized by adding finite amplitude perturbations to the initial data. These predictions can be tested with current experimental setups and might be other tests of the existence of purely dynamical instabilities in the two-condensate system of Ref. [15].

Of course the two-mode theory used here cannot be used to explain all the possible dynamical regimes of a real multicondensate system. In fact it is shown in Ref. [17] that depending on the perturbations applied to the system, spatiotemporally chaotic regimes may develop. These regimes cannot be handled with two modes. However, for many situ-

ations ranging from two-dimensional condensates to three-dimensional ones with small perturbations, the two-mode theory is a simple way to *understand* the complex dynamics of vortices in multicondensate systems. Indeed, the fact that such a simple model already provides the most interesting properties of the system is another proof of our statement that the instability of the $|0,1\rangle$ configuration is something essential to the dynamics of these condensates.

The proposed possibility of making the condensate in $|2\rangle$ stable or unstable by controlling the population ratio is interesting from the viewpoint of condensate engineering. We hope that this work helps in the task of understanding the complex dynamics of vortices in Bose-Einstein condensates.

ACKNOWLEDGMENT

This work has been partially supported by the DGICYT under Grant No. PB96-0534.

[1] P.G. Saffman, *Vortex Dynamics* (Cambridge University Press, Cambridge, England, 1997).
[2] Y. Kivshar and B. Luther-Davis, Phys. Rep. **298**, 81 (1998).
[3] A.M. Campbell and J.E. Evetts, Adv. Phys. **21**, 199 (1972); G. Blatter *et al.*, Rev. Mod. Phys. **66**, 1125 (1994).
[4] L.P. Pitaevskii, Zh. Éksp. Teor. Fiz. **40**, 646 (1961) [Sov. Phys. JETP **13**, 451 (1961)].
[5] D. Mermin, Rev. Mod. Phys. **51**, 591 (1979).
[6] M.H. Anderson *et al.*, Science **269**, 198 (1995); C.C. Bradley *et al.*, Phys. Rev. Lett. **75**, 1687 (1995); K.B. Davis *et al.*, *ibid.* **75**, 3969 (1995).
[7] R. Dum, J.I. Cirac, M. Lewenstein, and P. Zoller, Phys. Rev. Lett. **80**, 2972 (1998); K.-P. Marzlin, W. Zhang, and E.M. Wright, *ibid.* **79**, 4728 (1997); K.-P. Marzlin and W. Zhang, Phys. Rev. A **57**, 3801 (1998); M. Nakanara, T. Isoshima, K. Machida, S. Ogawa, and T. Ohmi, e-print cond-mat/9905374; B. Jackson, J.F. McCann, and C.S. Adams, Phys. Rev. Lett. **80**, 3903 (1998); K. Petrosyan and L. You, Phys. Rev. A **59**, 639 (1999).
[8] B.M. Caradoc-Davies, R. Ballagh, and K. Burnett, Phys. Rev. Lett. **83**, 895 (1999).
[9] F. Zambelli and S. Stringari, Phys. Rev. Lett. **81**, 1754 (1998); E. Lundhl, C.H. Pethick, and H. Smith, Phys. Rev. A **58**, 4816 (1998); E.V. Goldstein, E.M. Wright, and P. Meystre, *ibid.* **58**, 576 (1998); E.L. Bolda and D. Walls, Phys. Rev. Lett. **81**, 5477 (1998); F. Dalfovo and M. Modugno, Phys. Rev. A **61**, 023605 (2000).
[10] R.J. Dodd, K. Burnett, M. Edwards, and C.W. Clark, Phys. Rev. A **56**, 587 (1997); T. Isoshima and K. Machida, J. Phys. Soc. Jpn. **66**, 3502 (1997); A.A. Svidzinsky and A.L. Fetter, Phys. Rev. A **58**, 3168 (1998); A.L. Fetter, J. Low Temp. Phys. **113**, 189 (1998); H. Pu *et al.*, Phys. Rev. A **59**, 1533 (1999); T. Isochima and K. Machida, *ibid.* **59**, 2203 (1999).
[11] D.S. Rokhsar, Phys. Rev. Lett. **79**, 2164 (1997).
[12] J.J. García-Ripoll and V.M. Pérez-García, Phys. Rev. A **60**, 4864 (1999).
[13] M. Linn and A.L. Fetter, Phys. Rev. A **60**, 4910 (1999).
[14] B. Jackson, J.F. McCann, and C.S. Adams, Phys. Rev. A **61**, 013604 (2000).
[15] M.R. Matthews, B.P. Anderson, P.C. Haljan, D.S. Hall, C.E. Wieman, and E.A. Cornell, Phys. Rev. Lett. **83**, 2498 (1999).
[16] J. Williams and M. Holland, Nature (London) **401**, 568 (1999).
[17] J.J. García-Ripoll and V. M. Pérez-García, Phys. Rev. Lett. **84**, 4264 (2000).
[18] D.S. Hall, M.R. Matthews, J.R. Ensher, C.E. Wieman, and E.A. Cornell, Phys. Rev. Lett. **81**, 1539 (1998).
[19] O. Gómez-Calderón, V.M. Pérez-García, I. Martín, and J.M. Guerra, Phys. Rev. A **53**, 3490 (1996).
[20] One might think that our analysis works on the unstable manifold of the problem, which can be described with a space of a much lower dimensionality than the whole problem.
[21] The evolution of the phase singularities can be obtained from the condition $\mathrm{Re}(\psi_j)=\mathrm{Im}(\psi_j)=0$. The position of the phase singularity at $|2\rangle$ is given by the equations $x_s(t)=|a(t)|\sin[\phi_a(t)-\phi(b)+\pi]/|b(t)|$, $y_s(t)=|a(t)|\cos[\phi_a(t)-\phi(b)+\pi]/|b(t)|$.